FePt Icosahedra with Magnetic Cores and Catalytic Shells

Rongming Wang,*,†,‡ Olga Dmitrieva,§ Michael Farle,§ Günter Dumpich,§ Mehmet Acet,§ Sergio Mejia-Rosales,|| Eduardo Perez-Tijerina,|| Miguel Jose Yacaman,⊥ and Christian Kisielowski‡

Department of Physics, Beijing University of Aeronautics and Astronautics, Beijing 100191, People's Republic of China, National Center for Electron Microscopy, Lawrence Berkeley National Laboratory, University of California, Berkeley, California 94720, USA, Fachbereich Physik and Center of Nanointegration (CeNIDE), Universität Duisburg-Essen, Lotharstr. 1, 47048 Duisburg, Germany, Universidad Autónoma de Nuevo León, Facultad de Ciencias Físico-Matemáticas, San Nicolás de los Garza, Nuevo León, México 66450, and Chemical Engineering Department, University of Texas-Austin, Austin Texas 78712, USA

Received: December 20, 2008; Revised Manuscript Received: January 22, 2009

Surprisingly oxidation resistant icosahedral FePt nanoparticles showing hard-magnetic properties have been fabricated by an inert-gas condensation method with in-flight annealing. High-resolution transmission electron microscopy (HRTEM) images with sub-Angstrom resolution of the nanoparticle have been obtained with focal series reconstruction, revealing noncrystalline nature of the nanoparticle. Digital dark-field method combined with structure reconstruction as well as HRTEM simulations reveal that these nanoparticles have icosahedral structure with shell periodicity. Localized lattice relaxations have been studied by extracting the position of individual atomic columns with a precision of about ±0.002 nm. The lattice spacings of (111) planes from the surface region to the center of the icosahedra are found to decrease exponentially with shell numbers. Computational studies and energy-filtered transmission electron microscopy analyses suggest that a Pt-enriched surface layer is energetically favored and that site-specific vacancies are formed at the edges of facettes, which was experimentally observed. The presence of the Pt-enriched shell around an Fe/Pt core explains the environmental stability of the magnetic icosahedra and strongly reduces the exchange coupling between neighboring particles, thereby possibly providing the highest packing density for future magnetic storage media based on FePt nanoparticles.

Introduction

The potential use of self-assembled arrays of high-anisotropy magnetic FePt nanoparticles (NP) in future data storage media has attracted significant research effort over the past few years. They have been synthesized using organometallic chemistry or gas-phase condensation methods. The latter method affords the possibility to form differently shaped nanoparticles like icosahedra, decahedra, and cuboctahedra, and also larger facetted spheres. The shape and crystal structure determines the magnetic anisotropy K of individual particles and hence their long-term magnetic stability when used as magnetic bits in recording media. The magnetic anisotropy density depends critically on the distortion of a magnetic cubic crystal and may increase by several orders of magnitude for strains of less than 2% as evidenced in the tetragonally distorted $L1_0$ phase of FePt. The transformation to this phase in FePt NPs smaller than 4 nm has never been unambiguously identified, and the possibility of its formation in small NPs has been questioned[1,2] based on the influence of surface composition and segregation.[3] Commonly in these discussions, a uniform crystal structure across the NP is assumed that is the influence of a possible relaxation of the surface layers as is known at the surface of bulk crystals is not considered. Here, we show that the layer-resolved surface relaxations of a few percent indeed exist in icosahedral FePt NPs, which may be driven by the formation of Pt-enriched surface layers.

Icosahedral shaped NPs, which have been synthesized in this work by a gas-phase method can be described as a platonic solid in which each tetrahedron was distorted[4] and defects such as partial dislocations are present.[5] Such noncrystallographic structures were called multiply twinned particles or MTPs.[6]

There are substantial debates as to their growth mechanism.[5] Recently, increasing evidence reveals that nanoparticles and clusters possess shell periodicity and grow by the accretion of atomic layers.[7] The shell periodicity imposes certain restrictions on the symmetry of the clusters following Plato's five geometric bodies.[8−10] Excellent examples of such shell structures are Mackay icosahedra,[11] which are composed of 20 twin-related tetrahedra packed along (111) faces. Elastic deformation of the individual tetraheda is required, if merged into icosahedra, which is why one expects that such particles be compressed. However, despite intensive studies on its structure, no direct experimental evidence for such a structural shell from atomically resolved images has been reported before. The problem is the limitation of previous transmission electron microscopy techniques and the instability of nanoparticles under high-energy electron beam irradiation.[12−14] Recently, we briefly reported a quantitative determination of the layer-resolved structural relaxation at the surface of FePt icosahedral nanoparticles by high-resolution transmission electron microscopy with focal series reconstruction with sub-Ångstrom resolution for the first time.[15] Here, more details of our investigation on the icosahedron structure of the

* To whom correspondence should be addressed. E-mail: rmwang@buaa.edu.cn.
† Beijing University of Aeronautics and Astronautics.
‡ University of California, Berkeley.
§ Universität Duisburg-Essen.
|| Universidad Autónoma de Nuevo León.
⊥ University of Texas-Austin.

10.1021/jp811280k CCC: $40.75
Published on Web 02/25/2009

FePt nanoparticle together with molecular dynamics calculations are reported, which confirm the possible existence of a Pt-enriched surface layer. In the calculation, it is demonstrated that the segregation of Pt to the surface and the formation of site-specific vacancies at the edges of facettes is energetically favored, which was experimentally observed.

Experimental Section

FePt nanoparticles with diameters of 5−6 nm were formed in the gas phase in a DC-sputtering process in a continuous gas flow of Ar and He.[16] This approach forms the particles first and then accomplishes a sintering step (T_s = 1073 K), whereas the particles are still in the gas phase. To prevent the particles from oxidation during formation, the whole equipment is designed to meet ultra-high vacuum standards. Argon (99.999%) and helium (99.999%) pass a two-stage cleaning facility consisting of oil filters and oxygen getters prior to being fed to the gas inlet of the sputtering chamber. An alloy target with a composition of $Fe_{55}Pt_{45}$ was used. The composition of individual particles was found to be $Fe_{52}Pt_{48}$ with error bars of less than 2%, as determined by EDAX. For the production of icosahedra, the gas pressure was adjusted to 0.5 mbar. The icosahedral structure was found to be stable up to an in-flight sintering temperature of T_s = 1273 K − the maximum achievable temperature. Gas-phase condensation at higher inert gas pressures up to 2 mbar increased the number of decahedral particles whose lattice can be transformed to the $L1_0$ phase upon annealing to 1273 K. At room temperature, the maximum flow rates for argon and helium are $\rho_{max,Ar} = \rho_{max,He} = 1.71\ s^{-1}$. The sputtering gun was driven at a constant dc power of P_{dc} = 250 W. Depending on the gas flow rate, the residence time of the particles within the hot zone of the sintering oven is 0.05 s $\leq \tau_s \leq$ 0.9 s. In the deposition chamber, the particles are deposited onto a liquid nitrogen cooled substrate holder.

TEM samples were prepared by direct deposition on a TEM grid in the nucleation chamber. Focal series of high-resolution TEM lattice images were recorded with a Philips CM300 FEG/UT instrument and reconstructed with the *True-Image* professional 1.0.1 software[17,18] to obtain exit waves. A resolution of 0.08 nm can be obtained this way.[19] Image simulations were carried out with the *MacTempas* software.[20] Finally, we pinpoint atom column positions by fitting model functions to the intensity maxima of electron exit waves (phase images) with a precision of 0.1 pixel.[21] At the magnification used here, this corresponds to a precision of 0.002 nm that coincides with the precision as to which the lattice images are aligned during the exit wave reconstruction, which is a limiting factor. Energy-filtered TEM analyses were conducted in a 200 kV FEI monochromated Tecnai F20 UT microscope.

To compare with our experimental results with theory, molecular dynamics simulations were utilized. A Sutton−Chen (SC) many-body interatomic potential was used in the constant temperature ensemble (NVT), a Verlet algorithm was used for the integration of Newton's equations of motion, and a time step of 1.5 fs was employed.[9]

Results and Discussions

Such icosahedral FePt NP had shown a remarkable resilience against the phase transformation into the thermodynamically favored $L1_0$ phase even when annealing to 1273 K in the gas phase.[22] Only after annealing to 1273 K on a carbon substrate, $L1_0$ building blocks could be identified in larger decahedral particles that had formed by agglomeration of the MTPs. Furthermore, recent X-ray absorption studies[23] showed a surprisingly small oxide contribution in the $L_{3,2}$ near-edge spectra of Fe when compared to chemically prepared FePt NPs. In this article, we provide further evidence on the exceptional structural stability even under high-energy electron beam illumination and demonstrate that the formation of a surface-enriched Pt layer associated with a surface-layer relaxation prevents the formation of the $L1_0$ phase and provides an oxidation resistant layer in icosahedral NPs.

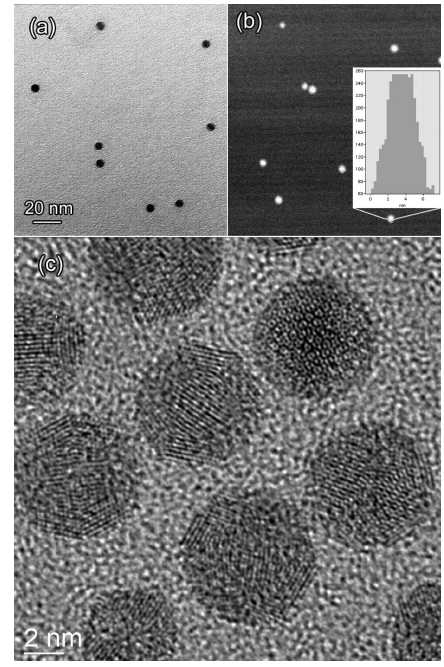

Figure 1. Microstructure and distribution of the FePt nanoparticles. (a) Standard bright-field TEM of the nanoparticles on carbon support films show homogenously distributed particles with identical sizes of about 5−6 nm. Different diffraction contrasts and shapes are due to the complex structure nature of the nanoparticles. (b) Z-contrast STEM image and image intensity line profile (inset) across one particle of FePt nanoparticles, showing lower intensity around the edges of the nanoparticle. (c) Standard HRTEM images of the nanoparticle showing distinct lattice fringes and straight edges.

Bright-field TEM, Z-contrast scanning TEM (STEM), and high-resolution TEM (HRTEM) images of the nanoparticles on carbon support films show homogenously distributed particles with identical sizes of about 5−6 nm. As shown in part a of Figure 1, the bright-field TEM image shows different diffraction contrasts and shapes, which are due to the different orientations of the nanoparticles. It also implies that the nanoparticles have a complex structure. The Z-contrast (STEM) image of FePt nanoparticles (part b of Figure 1) shows bright contrast, which is related to the atomic numbers of the atoms and the thickness of the sample. In the bright field TEM image, we can find a peculiar diffraction contrast, which is similarly observed in the STEM images showing a lower contrast around the edges than in the center. The inset of part b of Figure 1 depicts a typical image intensity line profile across one representative nanoparticle, showing lower intensity around the edges of the nanoparticle. This indicates that at surface facets fewer atoms are in the atomic columns along the electron beam or the atoms near the particles' surface are lighter. HRTEM images of the nanoparticle show distinct lattice fringes and straight edges. These are not typical for single-crystal particles for which the parallel lattice fringes should pass through the entire particle. The fringes in part c of Figure 1 show different fringe structure and the parallel fringes only partially exist. Each particle consists of several such parallel fringes. Such phenomena cannot be

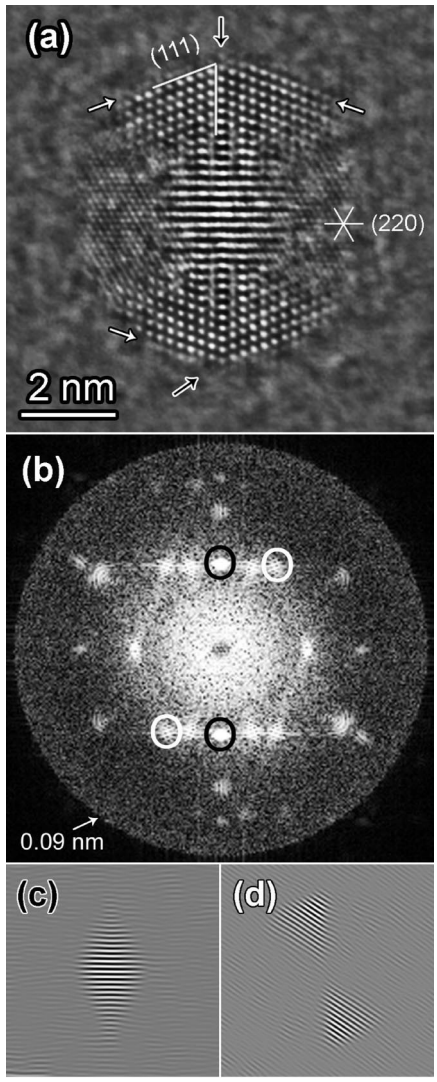

Figure 2. Exit wave phase image (a), fast Fourier transform (b), and two representative digital dark-field images (c,d) of one FePt nanoparticle. In part a, the white arrows mark partly occupied shells and the dark arrows mark edge columns that are commonly missing. Part b shows information transfer at an information limit of 0.090 nm. Parts c and d show butterfly-like or triangular contrast, showing the multiply twinning nature of the particle.

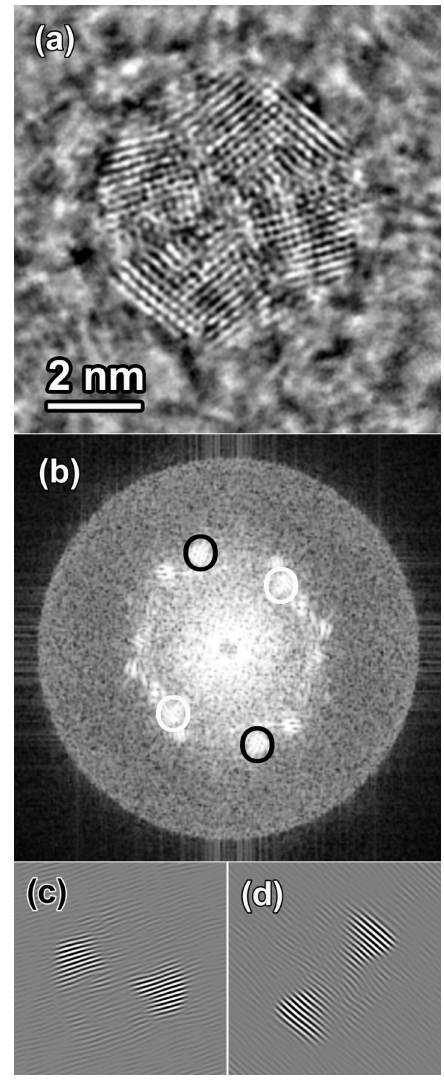

Figure 3. Exit wave phase image (a), fast Fourier transform (b), and two representative digital dark-field images (c,d) of another FePt nanoparticle. Despite of different fringes between the phase images in part a of Figure 2 and part a of Figure 3, the digital DF images show similar butterfly-like or triangular contrast, confirming the identical multiply twinning nature of the particles.

explained in the frame of a single crystalline particle. Because of limited resolution in part c of Figure 1 restricted by the spherical aberration of the objective lens, it is hard to get further information from the conventional TEM and HRTEM images.

Recent advances in TEM imaging approaches such as the reconstruction of electron exit waves from focal series of lattice images extend the resolution to the sub-Ångstrom regime to correct for dominant aberrations of the objective lens.[19,24] Figures 2 and 3 show exit wave phase images of two representative FePt nanoparticles that were reconstructed from two focus series, each consisting of 20 lattice images. In total, about 20 icosahedra of equal size were analyzed in the same extensive way by two different microscopists, and the same results were obtained within the reported experimental error.

In the reconstructed phase images, the intensity maxima mark atom columns that can be analyzed in terms of column positions and heights (sample thickness). The low intensities indicate that the corresponding atomic columns are only partially filled, as indicated by white arrows in part a of Figure 2. The intensities of edge columns (marked by black arrows in part a of Figure 2) are much lower or even absent, proving that whole columns can be removed from these sites.

The lattice fringes can be observed throughout the entire nanoparticle with sub-Ångstrom resolution. Because of the special fringe structure in part a of Figure 2 and part a of Figure 3, we assume the structure to be one of MTPs instead of single crystals.

The acquisition time for one focal series of 20 lattice images was ~100 s. The current density at the sample was measured to be ~20 A/cm^2 at 300 kV. It is remarkable to find that under such conditions the FePt nanoparticle was stable. Moreover, the large particle stability allows for a record resolution around 0.1 nm. The fast Fourier transformation in part b of Figure 2 demonstrates that the outer circle marks an information limit of 0.090 nm. Image Fourier components extend to this limit. It follows that sub-Ångstrom resolution can be not only from suitably prepared bulk materials[25] but also from complex, nonperiodic atom column positions in nanostructures.

Following the experimental dark-field method used by Ino,[6] digital dark-field (DF) methods by windowing different pairs of spots in the fast Fourier transformation (FFT) image of the

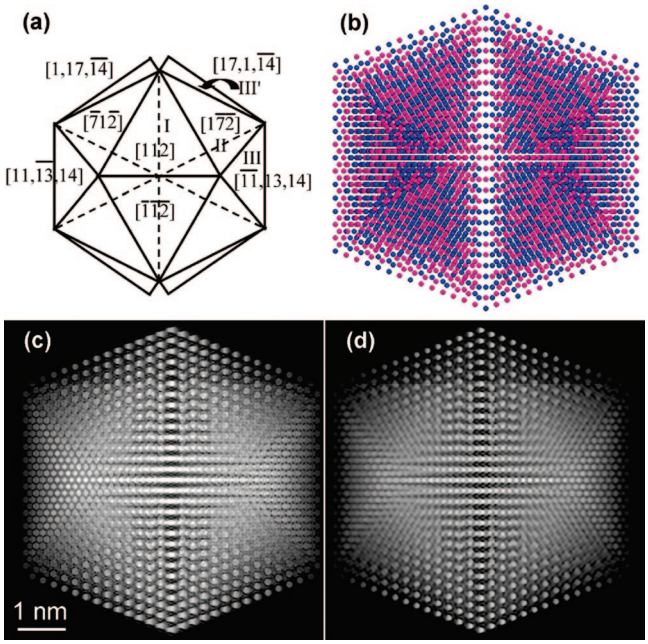

Figure 4. Icosahedron structures of the FePt nanoparticle in part a of Figure 2. (a) Diagram of MT model of tetrahedrons from ⟨112⟩ orientation to ⟨110⟩ and ⟨111⟩ orientations, (b) proposed shell growth icosahedron model with 10 179 randomly distributed Fe and atoms. Red and blue circles represent Fe and Pt atoms, respectively. (c) Simulated phase image from part b. (d) Simulated phase image from MT model relaxed by energy minimization. Both simulations prove that the particle is an icosahedral MTP.

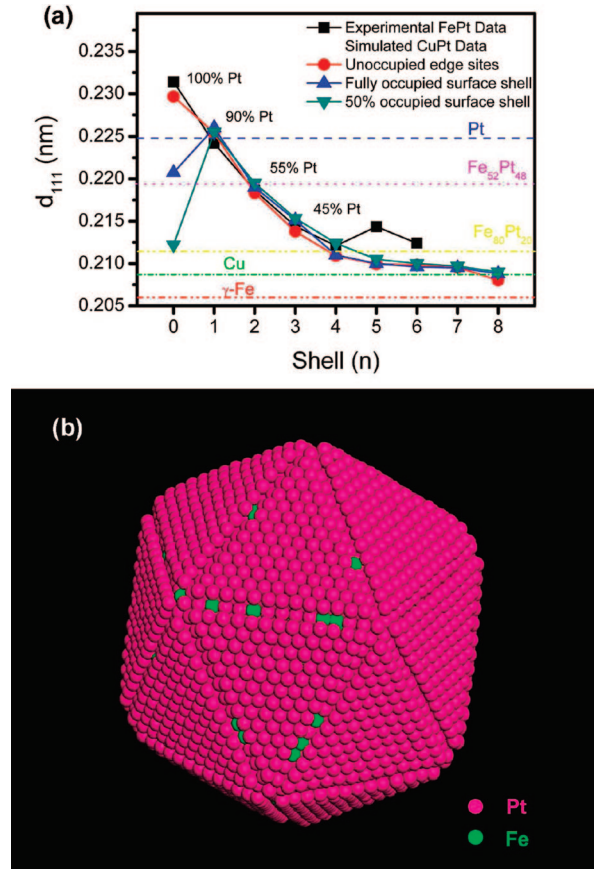

Figure 5. (a) Comparison of experimentally measured (FePt) and simulated (CuPt) shell spacing. Element segregation as discussed in the text can explain the exponential lattice relaxation to create a Pt shell and a Fe (Cu) rich core. The simulations show that randomly distributed surface vacancies contribute to a partial strain relaxation. Missing edge atoms in the topmost layer ($n = 0$) are required (full pink dots) to match the experimental result. (b) Proposed icosahedron 10 179 atom sites and Pt atoms that segregated to the surface (pink). Edge atom columns are removed making some of the (green) iron atoms of the second shell visible.

HRTEM were applied to obtain part a of Figure 2 and part a of Figure 3. The FFT and corresponding digital DF images are illustrated in parts b−d of Figure 2 and in parts b−d of Figure 3. Despite different fringes in part a of Figure 2 and part a of Figure 3, the digital DF images show similar butterfly-like or triangular contrast, which implies the identical multiply twinning nature of the particles.

The images of part a of Figure 2 show well-resolved {111} and {220} planes with spacing of 0.220 and 0.135 nm of the fcc FePt structure (space group $Fm3m$, $a = 0.3816$ nm). The 0.135 nm {220} lattice spacing is below the 0.168 nm point resolution of the instrument. The upper and lower parts of the phase are structural projections of tetrahedra viewed along the ⟨110⟩ directions, whereas the left and right parts correspond to views along ⟨111⟩ directions. The complex fringes in the center were determined as belonging to a projection along ⟨112⟩.

The above directions can be explained in the frame of icosahedrons. Part a of Figure 4 shows the diagram of multiply twinning of tetrahedrons from ⟨112⟩ to ⟨110⟩ and ⟨111⟩. Tetrahedrons along [112] (marked as I in part a of Figure 4) and [$\bar{1}\bar{1}2$] forms the first twinning. The second twinning of the tetrahedron along [112] is orientated along [$1\bar{7}\bar{2}$] (marked as II in part a of Figure 4). Analogies give higher order twinning of tetrahedrons along ⟨11,13,14⟩ and ⟨1,17,14⟩. The misfit between [−11,13,14] (marked as III in part a of Figure 4) and [−1,1,1] is calculated to be 5.6° and that between [17,1,−14] (marked as III′ in part a of Figure 4) and [1,0,−1] is 6.1°, which is in accordance with the nature of icosahedron with six angular gap or wedge Volterra declinations running through the particle along the directions joining the apexes of an icosahedron to the center.[5]

Digital DF methods and geometry constructions from the reconstructed phase images reveal that the particle structure described above must be interpreted in terms of a multiply twinned (MT) model. Initially, the 10 179 Fe and Pt atoms were distributed statistically according to their chemical ratio (52:48) to simulate a phase image. There are two approaches to construct an icosahedron. The geometrical structure model of part a of Figure 4 can either have a shell growth model[5] (part b of Figure 4) or be relaxed by energy minimization.[9] Red and blue circles in part b of Figure 4 represent Fe and Pt atoms, respectively. The corresponding simulated phase images of exit waves are shown in parts c and d of Figure 4. Both approaches yield phase images that compare well with the experimental phase image of part a of Figure 2, which proves that the particle is an icosahedral MTP. Residual differences relate to an imperfect alignment of the particles zone axis with the electron beam.

A quantitative evaluation of strain relaxation processes is possible by extraction of column position maps from the experiments. Here, one must also consider the possibility that there may be buckling of atoms in the atomic columns that might cause an anisotropic smearing of the intensity profile of the respective column. Within our resolution, such anisotropic intensity is not observed, and we can recover the centers of such columns from the experiment by fitting model functions to intensity maxima. The spacing between shells n and $n + 1$ in part a of Figure 2 is plotted in part a of Figure 5, where $n = 0$ marks the difference between the outermost and the first shell,

which is 0.231 ± 0.004 nm. It indicates that a smaller occupancy of the outermost layer results in a larger spacing. It is most unexpected to see in part a of Figure 5 that the spacing between the shells decreases exponentially with shell numbers. It can be described as:

$$d_{111}(n) = 0.2113 + 0.0204e^{-n/1.8}\ \text{nm} \qquad (1)$$

Eq 1 results in ~9.4% outward relaxation of the surface layer ($n = 0$) when compared to the spacing of the inner layers $n =$ 3 to 6. Comparison with the lattice structure of fcc $Fe_{52}Pt_{48}$ ($d_{111}^{fcc} = 0.2198$ nm) reveals that the surface is under tensile strain by 6% and the inner shells ($d_{111} = 0.213$ nm) are compressed by 3%.

To understand the reason for the outward relaxation and the compression inside the core, we performed molecular dynamics simulations using CuPt as a model system. Cu has a similar size as Fe, and the calculated structural relaxation results are expected to be the same for FePt. Every simulated particle was defined starting from a perfect icosahedron of 1079 atoms. The particle was thermalized at 300 K by a NVT molecular dynamics preliminary run, using no restrictions on the geometry nor on the atomic arrangement, for a number of steps large enough to stabilize the average configurational energy. Once thermalized, we proceed with the production run without any change in the parameters. The calculated lattice spacing in (111) orientation is also shown in part a of Figure 5. It is seen that the bulk lattice parameter of the smaller element is approached toward the core of the model particle. This process reduces compressive strain. At the particles surface, however, the experimental and the calculated d_{111} spacings even exceed the bulk lattice parameter of solid Pt. Such dependence can partly be explained if the particle is Fe (Cu) rich at its core and Pt covered at the surface, which requires element segregation. The indicated percentage values give the relative concentration of the respective Pt occupation of individual shells. Interestingly, the calculations shows that the outermost shell ($n = 0$) is largely compressed when one assumes perfect facets. This is in disagreement with the experiment. This discrepancy cannot be explained by a random loss of atoms from the outer shell (part a of Figure 5) as shown by the calculation 50% of the CuPt surface layer atoms are randomly removed. Instead, the simulations require a site-specific atom loss or vacancy formation at the edges of the merging {111} planes in the outermost shell ($n = 0$) must be present. Preferential absence of atoms at these sites is indeed what we observe in our experiments (indicated by black arrows in part a of Figure 2). The calculation also indicates that at most the one or two topmost layers are Pt enriched. Part b of Figure 5 shows an idealized model of our findings that disregards a possible partial substitution of iron atoms in the outermost shell. The presence of such a Pt-enriched surface layer provides a natural explanation for the experimentally observed oxidation resistance of the MTPs in comparison to colloidal FePt particles.

Energy-filtered TEM (EFTEM) analysis also confirms that FePt particles have Fe-rich cores and Pt-rich shells. Figure 6 shows a typical EFTEM result of the nanoparticle. Parts a and b of Figure 6 show ion pre-edge and post-edge images of the nanoparticles, respectively. Part c of Figure 6 shows a calculated ion map of the nanoparticles. Quantitative comparison is performed by depicting image intensity line profiles across the same nanoparticle (indicated by a white arrow), as shown in parts d and e of Figure 6. It can be seen that the brightness for the nanoparticles in the center in parts a and b of Figure 6 is relatively higher than those along the edges. The iron mappings of the nanoparticles in part c of Figure 6 show smaller particle sizes. Compared with the nanoparticle sizes of ~5 nm in part a of Figure 6, the iron mapping sizes of the nanoparticles is only ~4 nm with about two shells smaller, which matches the theoretical predictions in part b of Figure 5.

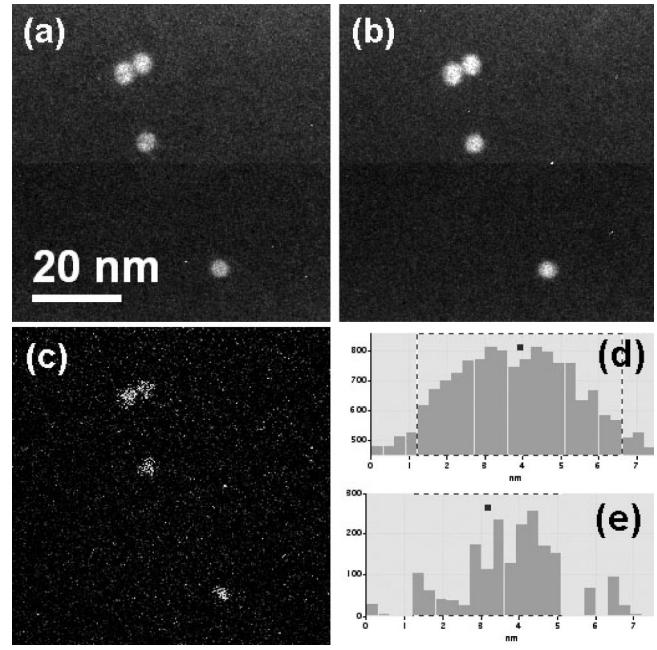

Figure 6. EFTEM of FePt nanoparticle. (a) Iron Pre-edge image, (b) Iron Postedge image, (c) Iron mapping, (d,e) image intensity line profiles across the nanoparticle indicated by white arrow in parts a and c of Figure 6, showing smaller particle sizes in the iron mapping image.

The Pt segregation that according to the calculations and the experimental observations is energetically favored also prevents the formation of the $L1_0$ phase because the composition has become more Fe rich. Additionally, we want to mention another piece of evidence for the formation of the Pt shell. When we change the gas-phase synthesis parameters, we do not find the MTPs (Experimental Section). We rather observed decahedral particles that can be transformed to the $L1_0$ phase by annealing when we perform the synthesis at higher inert gas pressures or in other words higher ion etching rates. This prevents the formation of stabilizing Pt shells and leads to the observation of oxidized Fe in X-ray absorption spectra.

Conclusions

This article reports a detailed investigation of the formation of a shell periodic, icosahedral FePt particle with a resolution that breaks the 1 Å barriers. The particles are remarkably stable under electron beam irradiation. Quantitative analyses of displacement fields with a precision approaching picometer values reveals that the expected compressive strain in the particle relaxes by element segregation and a novel mechanism involving site-specific vacancy formation that is confirmed by molecular dynamics simulations. As a result, the composition of the icosahedral nanoparticles is inhomogeneous − possibly showing Fe−Pt structures with different Fe/Pt ratios with a Pt shell and a Fe-rich core, which makes them environmentally stable nanomagnets with a surface layer that suppresses unwanted exchange coupling effects when used as magnetic recording bits in magnetic ultrahigh density data storage and sensor applications.

Acknowledgment. This work was supported by the National Natural Science Foundation of China (No. 50671003), the

Program for New Century Excellent Talents in University (NCET-06-0175), the Director, Office of Science, Office of Basic Energy Science, of the U.S. Department of Energy under contract No. DE-AC02-05CH11231, the Berkeley Scholar Program, the Deutsche Forschungsgemeinschaft SFB 445, and the Council for Science and Technology of the State of Nuevo León, México.

References and Notes

(1) Antoniak, C.; Lindner, J.; Spasova, M.; Sudfeld, D.; Acet, M.; Farle, M.; Fauth, K.; Wiedwald, U.; Boyen, H. G.; Ziemann, P.; Wilhelm, F.; Rogalev, A.; Sun, S. H. Phys. Rev. Lett. **2006**, *97*, 117201.

(2) Gruner, M. E.; Rollmann, G.; Entel, P.; Farle, M. Phys. Rev. Lett. **2008**, *100*, 087203.

(3) Muller, M.; Albe, K. Phys. Rev. B **2005**, *72*, 094203.

(4) Yacamán, M. J. *Review of Recent Progress in Surface Science*; Vanselow, R., Ed.; Springer: New York, 1984; *35*, 183.

(5) Marks, L. D. *Rep. Prog. Phys.* **1994**, *57*, 603.

(6) Ino, S. *J. Phys. Soc. Jpn.* **1966**, *21*, 346.

(7) Sudfeld, D; Dmitrieva, O.; Friedenberger, N; Dumpich, G; Farle, M.; Song, C.-Y.; Kisielowski, C.; Gruner, M. E.; Entel, P. *Mater. Res. Soc. Symp. Proc.* **2007**, *998E*, 0998-J01−06.

(8) Martin, T. P. *Physics Reports-Review Section of Physics Letters* **1996**, *273*, 199.

(9) Rodriguez-Lopez, J. L.; Montejano-Carrizales, J. M.; Pal, U.; Sanchez-Ramirez, J. F.; Troiani, H. E.; Garcia, D.; Miki-Yoshida, M.; Jose-Yacaman, M. *Phys. Rev. Lett.* **2004**, *92*, 196102.

(10) Nam, H. S.; Hwang, N. M.; Yu, B. D.; Yoon, J. K. *Phys. Rev. Lett.* **2002**, 89.

(11) Mackay, A. L. *Acta Crystallogr.* **1962**, *15*, 916.

(12) Ajayan, P. M.; Marks, L. D. *Phys. Rev. Lett.* **1988**, *60*, 585.

(13) Iijima, S.; Ichihashi, T. *Phys. Rev. Lett.* **1986**, *56*, 616.

(14) Ajayan, P. M.; Marks, L. D. *Phys. Rev. Lett.* **1989**, *63*, 279.

(15) Wang, R. M.; Dmitrieva, O.; Farle, M.; Dumpich, G.; Ye, H. Q.; Poppa, H.; Kilaas, R.; Kisielowski, C. *Phys. Rev. Lett.* **2008**, *100*, 017205.

(16) Stappert, S.; Rellinghaus, B.; Acet, M.; Wassermann, E. F. *J. Cryst. Growth* **2003**, *252*, 440.

(17) Coene, W. M. J.; Thust, A.; deBeeck, M.; VanDyck, D. *Ultramicroscopy* **1996**, *64*, 109.

(18) Thust, A.; Coene, W. M. J.; deBeeck, M. O.; VanDyck, D. *Ultramicroscopy* **1996**, *64*, 211.

(19) Kisielowski, C.; Hetherington, C. J. D.; Wang, Y. C.; Kilaas, R.; O'Keefe, M. A.; Thust, A. *Ultramicroscopy* **2001**, *89*, 243.

(20) http://www.totalresolution.com/MacTempas.html.

(21) Kisielowski, C; Schmidt, O.; Yang, J. *Mater. Res. Soc. Symp. Proc.* **1998**, *482*, 369.

(22) Rellinghaus, B.; Stappert, S.; Acet, M.; Wassermann, E. F. *J. Magn. Magn. Mater.* **2003**, *266*, 142.

(23) Dmitrieva, O.; Spasova, M.; Antoniak, C.; Acet, M.; Dumpich, G.; Kastner, J.; Farle, M.; Fauth, K.; Wiedwald, U.; Boyen, H. G.; Ziemann, P. *Phys. Rev. B* **2007**, *76*, 064414.

(24) Jia, C. L.; Lentzen, M.; Urban, K. *Science* **2003**, *299*, 870.

(25) Xu, X.; Beckman, S. P.; Specht, P.; Weber, E. R.; Chrzan, D. C.; Erni, R. P.; Arslan, I.; Browning, N.; Bleloch, A.; Kisielowski, C. *Phys. Rev. Lett.* **2005**, *95*, 145501.

JP811280K